Dynamic Primitives Facilitate Manipulating a Whip

Moses C. Nah[1], Aleksei Krotov[2], Marta Russo[3], Dagmar Sternad[3,4] and Neville Hogan[1,5]

Abstract— **Human dexterity far exceeds that of modern robots, despite a much slower neuromuscular system. Understanding how this is accomplished may lead to improved robot control. The slow neuromuscular system of humans implies that prediction based on some form of internal model plays a prominent role. However, the nature of the model itself remains unclear. To address this problem, we focused on one of the most complex and exotic tools humans can manipulate—a whip. We tested (in simulation) whether a distant target could be reached with a whip using a (small) number of dynamic primitives whose parameters could be learned through optimization. This approach was able to manage the complexity of an (extremely) high degree-of-freedom system and discovered five optimal parameters of a single movement that achieved the task. An internal model of the whip dynamics was not needed for this approach, thereby significantly relieving the computational burden of task representation and performance optimization. These results support our hypothesis that composing control using dynamic motor primitives may be a strategy which humans use to enable their remarkable dexterity. A similar approach may contribute to improved robot control.**

I. INTRODUCTION

Tool-use is a hallmark of human behavior. The dexterity required to handle a broad range of tools has been widely recognized as a distinctively human characteristic [1]–[5]. Despite extensive research attempting to realize comparable dexterity in robots, the remarkable performance of humans has yet to be replicated, and a comprehensive theoretical framework remains to be established. A paradox emerges when we recognize that humans vastly out-perform modern robot technology despite low-bandwidth actuators, a high level of noise, and long latencies in neural communication within the neuromuscular system [6].

How does the human system perform so well despite its limitations? Rather than achieving motor skills based on real-time supervision and intervention from the central nervous system (CNS), the slow neuromuscular system implies that prediction based on some form of "internal model" plays a prominent role in human motor control [7]–[11]. In robotics, optimization is widely used for task planning, and optimization based on an internal model has successfully accounted for the coordination of simple reaching movements.

Although prediction is widely accepted as a key aspect of human motor control, the nature of the internal model itself remains unclear. To address this problem, we focused on one of the most complex and exotic tools which humans can manipulate—a whip. A whip is a flexible object with non-uniform mechanical properties that interacts with a compressible gas up to the supersonic regime. A competent engineering-style model to describe the whip dynamics requires nonlinear partial differential equations of infinite order [12], [13]. Due to what Richard Bellman called the "curse of dimensionality", the computational complexity of using optimization with an engineering-style model of whip dynamics is essentially unmanageable, taxing even modern super-computers. Nevertheless, apparently indifferent to this daunting complexity, humans can learn to manipulate a whip, sometimes with apparent ease, with some experts reaching an impressive level of spatial and temporal accuracy with the tip of the whip [14], [15].

This observation suggests that the CNS employs a fundamentally different approach than optimization based on an engineering-style model. Specifically, we suggest that humans simplify the task by composing motor control using dynamic motor primitives [16]–[20]. This term refers to dynamic behaviors that manifest as stable attractors of the (nonlinear) neuromechanical system. They are conceived as dynamic "building blocks" that may be combined to produce complex behavior. Three classes of dynamic primitives have been identified—submovements, oscillations and mechanical impedances, the latter to manage physical interaction—though there may be others.

We hypothesize that human motor control uses an internal representation that is solely encoded in terms of the parameters of dynamic primitives. Encoding motor tasks via parameterized dynamic primitives may dramatically simplify the control of complex object manipulation. Using optimization as a model of learning, this parameterization may enable convergence (or accelerate it) without encountering limitations due to the "curse of dimensionality".

This study tested (in simulation) whether a target could be reached with a whip using a (small) number of dynamic primitives, whose parameters were learned through optimization. We found that this approach was able to identify a single upper limb movement which approximated a distant target with a whip. This result supports our hypothesis that composing actions using dynamic motor primitives may be a strategy underlying human's remarkable dexterity. A similar approach may contribute to improved robot control.

Supported in part by NSF M3X-1826097 (Neville Hogan) and NSF M3X-1825942 (Dagmar Sternad), and NIH-R01-HD087089.

[1]Department of Mechanical Engineering, Massachusetts Institute of Technology, Cambridge, MA, USA

[2]Department of Bioengineering, Northeastern University, Boston, MA, USA

[3]Department of Biology, Northeastern University, Boston, MA, USA

[4]Department of Electrical and Computer Engineering, Department of Physics, Northeastern University, Boston, MA, USA

[5]Department of Brain and Cognitive Sciences, Massachusetts Institute of Technology, Cambridge, MA, USA

Email addresses: mosesnah@mit.edu, krotov.a@northeastern.edu, marta.russo.phd@gmail.com, d.sternad@northeastern.edu, neville@mit.edu

II. METHODS

The research presented in this paper used the simulation software MuJoCo [21], which provided a controlled environment to test our working hypothesis. For all of the MuJoCo simulations, the semi-implicit Euler method was chosen as the numerical integrator with a time step of 0.1 millisecond.

A. Modeling

The model used in the MuJoCo simulation consisted of two main parts: an N-node model of a whip (the object being manipulated) and a model of the human upper limb (the manipulator).

1) Model of a whip: An N-node "lumped-parameter" model was developed to approximate the continuum dynamics of a whip. It consisted of a finite sequence of serially-connected planar sub-models. Each sub-model was composed of three lumped-parameter elements: an (ideal) point mass, a linear torsional spring and a linear torsional damper. The point-mass $m\,[kg]$ was suspended from a single degree-of-freedom pivot with length $l\,[m]$. The pivot, a rotational joint, was equipped with a linear torsional spring and a linear torsional damper, with coefficients $k\,[N\cdot m/rad]$ and $b\,[N\cdot m\cdot s/rad]$, respectively. N of these identical planar sub-models were serially connected to comprise the N-node whip model. The parameters (N, l, m, k, b) will be called the "whip parameters" of the model.

2) Model of the human upper limb: The human upper limb was modeled as a two-bar open-chain linkage. The fingers, hand and wrist (everything distal to the wrist joint) were excluded from this model. The shoulder and elbow were modeled as single degree-of-freedom rotational joints. The shoulder joint axis was fixed in space, and the movement of the upper limb model was confined to the sagittal plane. Independently controlled torque actuators were mounted coaxially with the shoulder and elbow joints. The two limb segments were taken to be non-uniform cylinders, i.e. the center of mass and the geometric center of the segment were not identical. Assuming right-handedness, the geometrical and inertial parameters for each limb segment were derived from a computational model by Hatze [22], and detailed values are presented in Table I.

3) Combined model (whip + upper limb): The discretized N-node whip model was planarly connected to the two-segment upper limb model with a single degree-of-freedom rotational joint. No stiffness or damping elements were included for this rotational joint, i.e. a freely-rotating hinge was used for the connection. Summarizing, the combined model simulated a sequential open-chain planar mechanism with $N+2$ degrees-of-freedom.

B. Validation of the MuJoCo Simulator

To assess the reliability of the MuJoCo simulator, the total (kinetic+potential) energy of a lossless N-node whip model was computed. The lossless model was created by setting the torsional damping coefficient b to zero for the N sub-models. The simulation started with the whip in an equilibrium configuration, at rest hanging vertically downward. A single degree-of-freedom linear actuator, driven by a position controller with high proportional gain, moved the top of the modeled whip in a horizontal motion from rest with the following movement profile $p(t)$:

$$p(t) = \frac{A}{2}\left\{1-\cos\left(\frac{2\pi}{w}\cdot(t-t_0)\right)\right\} \tag{1}$$

where $A\,[m]$ is the amplitude of the motion profile, $t_0\,[s]$ is the time when the motion started and $w\,[s]$ is the duration of the motion; $t\,[s]$ is the time variable defined in the domain $[t_0,\, t_0+w]$. For times before and after this interval, the top of the whip remained at rest, i.e. $p(t)=0$.

For 5 minutes, the total energy of the lossless whip model was computed at each time step. The potential and kinetic energy of the whole system were called using innate MuJoCo functions.

C. Analysis of a Linearized Whip Model

Nonlinear Euler-Lagrange equations of motion were linearized about rest in the vertically-downward position, yielding the following state-space representation:

$$\dot{\vec{x}} = A\vec{x} := \begin{bmatrix} 0_{n\times n} & I_{n\times n} \\ -M_w^{-1}(K_w+G_w) & -M_w^{-1}B_w \end{bmatrix} \begin{bmatrix} \vec{q} \\ \dot{\vec{q}} \end{bmatrix} \tag{2}$$

where $M_w, B_w, K_w, G_w \in \mathbb{R}^{n\times n}$ are matrices of inertia, damping, stiffness and gravitational effects, respectively; $0_{n\times n}, I_{n\times n} \in \mathbb{R}^{n\times n}$ are the zero and identity matrices, respectively; the vector $\vec{q} \in \mathbb{R}^n$ denotes joint angles in relative coordinates; dots denote derivatives with respect to time; $A \in \mathbb{R}^{2n\times 2n}$ is the state matrix and $\vec{x} \in \mathbb{R}^{2n}$ is the state vector.

To study the effect of damping b on the whip dynamics, the real (dissipative) and imaginary (oscillatory) components of the eigenvalues of matrix A were evaluated for different values of damping b. To check whether the dynamic behavior of the whip shown in the simulation of Sec. II-B was consistent with the eigenvalue analysis, the angle data of the N^{th} joint (i.e. the angle of the last sub-model of the whip model) were extracted with a sampling frequency of 500Hz. Using the Fast Fourier Transform (FFT) of the Numpy python library, a spectral analysis was conducted on a segment of the data.

D. Experimental Estimation of Realistic Whip Parameters

Physical parameters of a commercially available 6-foot bullwhip were identified. The distal parts of the whip (fall and cracker) were removed, and 10 customized reflective markers were mounted at equal distances along its main part, a thong of 1.8m length. The top of the handle was attached to a pivot, and the whip was freely suspended. The tip of the whip was manually displaced 20cm horizontally from equilibrium and released to initiate small oscillations. Twelve Oqus cameras (Qualisys, Goetheborg, Sweden) recorded the 3D position of whip markers for 20 seconds at a sampling rate of 500Hz.

The 2D horizontal position of those markers was used to measure the frequency $f\,[Hz]$ of the oscillation. All analyses were conducted using MATLAB (Mathworks Inc., Natick,

MA). The dominant frequency values were averaged across markers. With the identified frequency f, the exponential decay time-constant τ_{decay} $[s]$ of the oscillation was calculated, using the position of the marker at the tip of the whip.

Since the trace of oscillation was not aligned with the x and y axis of the Qualisys Cartesian coordinate frame, the position data were rotated so that the starting position of the marker resided on the x axis. The rotated x position vs. time was curve-fit with the following function $c(t)$ to find the coefficient of exponential decay τ_{decay}:

$$c(t) = Ce^{-t/\tau_{decay}} \sin(2\pi ft + \phi) \tag{3}$$

where C $[mm]$ is the amplitude and ϕ $[rad]$ is the phase offset of the sine function. The values of C, τ_{decay} and ϕ which minimized the sum of squared errors with the experimental data were searched. The mass m and length l parameters of the whip model were derived from the measured mass f $[Hz]$ (0.3kg) and length (1.8m) of the actual whip. Based on the frequency f and the exponential decay time-constant τ_{decay}, the stiffness k and damping b values of the whip model were computed to yield the same damped oscillation. The whip model with parameters derived from the experimental data will be called the "experimentally-fitted" whip model.

E. Control of the Upper Limb

1) Impedance controller: To account for physical interaction between the upper limb and the whip, the model included an impedance controller. The two-joint manipulator muscle model from Flash [23] was adopted and reconfigured:

$$\vec{\tau} = K(\vec{\phi} - \vec{\theta}) + B(\dot{\vec{\phi}} - \dot{\vec{\theta}}) + \vec{\tau}_G \tag{4}$$

In this equation, $K \in \mathbb{R}^{2\times 2}$ is a constant joint stiffness matrix, $B \in \mathbb{R}^{2\times 2}$ is a constant joint damping matrix, both representing the neuromuscular mechanical impedance of the upper limb [24]; vector $\vec{\tau}(t) = [\tau_1(t),\ \tau_2(t)]^T$ denotes the net torque input on each joint; subscripts 1 and 2 denote shoulder and elbow, respectively; vector $\vec{\tau}_G(t) = [\tau_{1,G}(t),\ \tau_{2,G}(t)]^T$ denotes the torque required for gravity compensation; vector $\vec{\theta}(t) = [\theta_1(t),\ \theta_2(t)]^T$ denotes the actual joint angle trajectory defined in relative angle coordinates; vector $\vec{\phi}(t) = [\phi_1(t),\ \phi_2(t)]^T$ represents a motion command from the CNS as a "zero-torque" trajectory, i.e. neglecting gravitation effects, if the actual joint angle trajectory $\vec{\theta}$ exactly matches the zero-torque trajectory $\vec{\phi}$, no torque will be exerted by the actuators. Gravitational effects were compensated with $\vec{\tau}_G$, so that the actual upper limb posture $\vec{\theta}$ could exactly match the zero-torque posture $\vec{\phi}$ when the whole model is at rest. The neuromuscular mechanical impedance parameters K and B were chosen to be positive definite symmetric matrices, and joint damping B was chosen to be proportional to joint stiffness K, such that $B = \beta K$ where β is a time-constant. Detailed values for K and B were borrowed from Flash [23], and are listed in Table I.

2) Zero-torque trajectory: The zero-torque trajectory of the upper limb model followed a rest-to-rest minimum-jerk profile [25] in joint coordinates:

$$\begin{aligned} \phi_1(t) &= \phi_{1,i} + (\phi_{1,f} - \phi_{1,i}) \cdot (10\tau^3 - 15\tau^4 + 6\tau^5) \\ \phi_2(t) &= \phi_{2,i} + (\phi_{2,f} - \phi_{2,i}) \cdot (10\tau^3 - 15\tau^4 + 6\tau^5) \end{aligned} \tag{5}$$

where $\tau := t/D$ is a normalized time variable defined on the domain [0, 1]; D is the duration of a single upper limb movement; t is time and subscripts i and f denote the initial and final postures, respectively. For times greater than the duration D (i.e. $t > D$), the zero-torque trajectory of the shoulder and elbow joint remained at $\phi_{1,f}$ and $\phi_{2,f}$, respectively.

3) Implementation: In the simulation, $\vec{\phi}(t)$ was determined by 5 movement parameters: ($\phi_{1,i}$, $\phi_{2,i}$, $\phi_{1,f}$, $\phi_{2,f}$, D). At every time step, the actual joint angle $\vec{\theta}$ and angular velocity $\dot{\vec{\theta}}$ for each joint were called from the simulation. Based on these values, the position and velocity deviation between the zero-torque trajectory $\vec{\phi}(t)$ and the actual joint angle trajectory $\vec{\theta}(t)$ were calculated. With the specified K and B matrices and the gravity compensation torque $\vec{\tau}_G$, the resultant torque values were calculated and applied to each torque actuator.

F. The Whip Task and Optimization

The objective of the whip task was to minimize the value L $[m]$, the distance between the tip of the whip and a target. To avoid chaotic behavior due to the model whip colliding with a target, the target was located at a distance just 0.01 m beyond the combined length of the upper limb and whip. The minimum value of the distance L reached with a single discrete (i.e. rest-to-rest) upper limb movement, L^* $[m]$, was a quantitative measure to assess performance. The distance L was calculated for each time step, by calling the Cartesian positions of the target and the tip of the whip from the simulation. Four variants of the whip model were tested: short, medium, long and experimentally-fitted. Detailed values of the whip parameters (N, l, m, k, b) are listed in Table II.

For each whip model, the optimal 5 movement parameters ($\phi_{1,i}$, $\phi_{2,i}$, $\phi_{1,f}$, $\phi_{2,f}$, D) which minimized L^* were identified with the nlopt (nonlinear optimization) C++ tool box. Within the global derivative-free optimization algorithm, the DIRECT-L (DIviding RECTangles, Locally biased) algorithm was chosen for the optimization [26]. The optimization process comprised 600 iterations.

III. Results

A. Numerical Dissipation of the MuJoCo Simulator

The energy of a lossless N-node whip model should remain constant after the excitation ended (Eq.1). However, using the (semi-implicit) Euler method as the numerical integrator in the MuJoCo simulation, a gradual decrease of total energy was observed. For models with more than one degree of freedom ($N > 1$), the simulated energy loss was pronounced (Fig. 1). This apparent dissipation of total energy, due to the accumulation of numerical error, acted as an "innate damper" in the simulation.

TABLE I: Parameters for Upper Limb Model [22], [23]

	Description	Notation	Values	Unit
Limb Inertia Parameters	Mass of Limb Segment	M_1, M_2	1.595, 0.869	$[kg]$
	Length of Limb Segment	L_1 , L_2	0.294, 0.291	$[m]$
	Length from proximal joint to Center of Mass	L_{c1}, L_{c2}	0.129, 0.112	$[m]$
	Moment of Inertia of Limb Segment w.r.t. Center of Mass	I_1 , I_2	0.012, 0.005	$[kg \cdot m^2]$
Neuromuscular Impedance	Stiffness Matrix K Elements	K_{11}, K_{12}, K_{22}	29.50, 14.30, 39.30	$[N \cdot m/rad]$
	Damping Matrix B Elements	B_{11}, B_{12}, B_{22}	2.950, 1.430, 3.930	$[N \cdot m \cdot s/rad]$

Subscripts denote the shoulder and elbow joints, numbered proximal to distal.

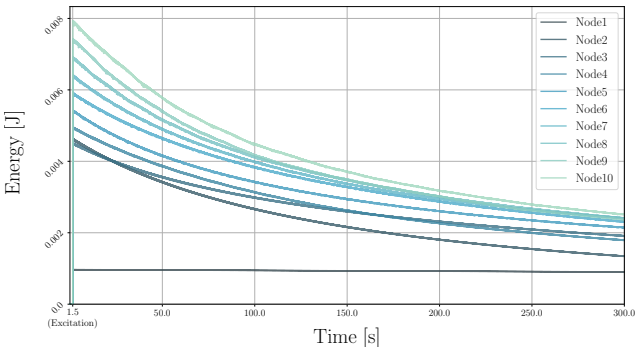

Fig. 1: Numerical dissipation of total energy over time with different lossless whip models. Values for mass m, length l, torsional stiffness coefficient k and torsional damping coefficient b were fixed and different values of node number N were tested. Whip parameters: (l, m, k, b) = (0.1, 0.02, 0.05, 0); displacement function parameters: (A, t_0, w) = (0.02, 1.5, 0.1).

B. Eigenstructure Analysis of the Whip Model

With the same damping coefficient b for all segments of the whip model, eigenvalues located further from the origin of the complex plane had proportionally larger real (dissipative) components. This pattern was observed for different values of b (Fig. 2a) . As a result, (eigen)modes with higher frequency decayed faster than (eigen)modes with lower frequency. In other words, high-frequency oscillatory behavior of the damped whip model quickly faded, and the whip was dominated by (eigen)modes with the lowest frequencies.

This theoretical result was confirmed by spectral analysis of the numerical simulation of a 3-node whip model. When a non-zero damping coefficient value b was included in the whip model, the dominant dynamic behavior was a single frequency of oscillation, which is shown as a single dominant peak in the power spectrum (Fig. 2b). The dominant frequency value of the numerically-simulated damped whip model was 1.175Hz, which was in reasonable agreement with the theoretical value for this parameter set, 1.168Hz. This result confirmed that, despite its limitations, with modest values of damping the simulation yielded plausible results.

C. Experimentally Identified Whip Parameters

The experimentally-observed frequency of whip oscillation f was 0.45Hz, and the exponential decay time-constant τ_{decay} was 29.24s. Choosing the number of nodes N as 25, the whip model parameters which reproduced the same oscillation frequency and exponential decay time-constant were determined. Detailed parameters of the experimentally-fitted whip model are presented in Table II.

D. Optimization Result

For each whip model, the DIRECT-L algorithm converged to an optimal set of five movement parameters which yielded the minimum value of distance L^* for the corresponding whip model. Detailed values of the optimal parameter set ($\phi_{1,i}$, $\phi_{2,i}$, $\phi_{1,f}$, $\phi_{2,f}$, D), and its corresponding output L^*, are presented in Table II. Representative movement profiles generated by the simulation with the optimal movement parameters are shown in (Fig. 3).

IV. Discussion

This study examined whether a target could be reached with a simulated whip using a (small) number of dynamic primitives, whose parameters could be learned through optimization. Because of the dynamic complexity of the whip model, this simple task is anything but trivial. It was not *a priori* obvious that the optimization would even converge, let alone produce a meaningful result. By encoding upper limb action using the parameters of dynamic primitives, the acquisition of the motor skill to achieve this task was greatly simplified. Simplifying the motor task via parameterized dynamic primitives dramatically reduced the computational complexity of the optimization problem, providing a way to work around the "curse of dimensionality". This approach successfully managed the complexity of an (extremely) high degree-of-freedom system (a 54^{th} order model for the highest degree-of-freedom whip model). In fact, a minimum distance from the target was achieved with a single discrete movement, defined by five parameters.

A. Relation to Prior Work

A growing body of evidence indicates that the human sensory-motor control system relies on a composition of primitives [16], [27]–[33]. In addition, dynamic movement primitives have successfully been used in robotics [34], [35]. Schaal et al. used movement primitives to learn from a demonstrated trajectory [36], and Peters and Schaal showed that a robotic arm was able to learn baseball via movement

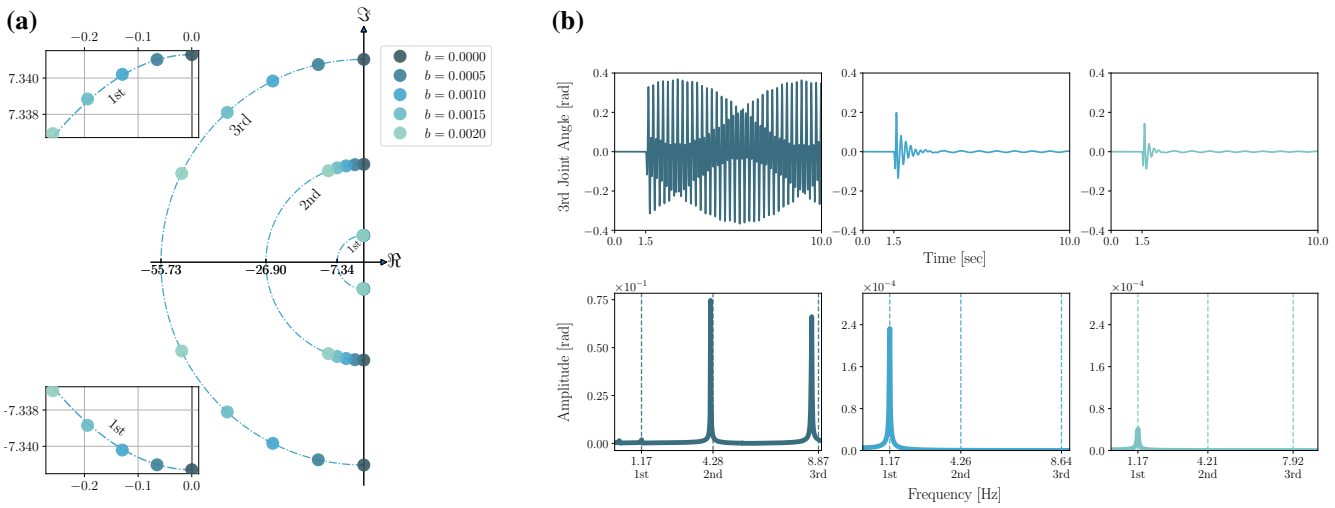

Fig. 2: (a) Plot of the eigenvalues of matrix A in the complex plane. The radial grids are numbered in ascending order of distance from the origin. Whip parameters: (N, l, m, k) = (3, 0.1, 0.02, 0.05). (b) Spectral analysis of a 3-node whip model. First row: time vs. 3^{rd} joint angle plot; second row: power spectra of the corresponding joint angle.The excitation of the whip model started at 1.5s. Within the 5 minute long data, spectral analysis was conducted on a segment of joint angle data from 20s to 60s. Columns show results with different values of joint damping; left to right, $b = 0$, 0.0005 and 0.001, respectively. Note the rapid convergence to a low-frequency oscillation with modest values of damping. The vertical dotted lines indicate the theoretical frequencies of the eigenmodes. Whip parameters: (N, l, m, k) = (3, 0.1, 0.02, 0.05).

TABLE II: Whip Type, Whip Parameters and Optimization Result

Type of Whip	Whip Parameters					Optimal Movement Parameters					Minimum Distance L^*
	N	l	m	k	b	$\phi_{1,i}$	$\phi_{2,i}$	$\phi_{1,f}$	$\phi_{2,f}$	D	
Short whip	10	0.10	0.10	0.05	0.005	−1.312	1.670	1.565	0.000	0.667	0.032
Medium whip	15	0.10	0.10	0.05	0.005	−1.447	0.368	1.562	0.121	0.833	0.048
Long whip	20	0.10	0.10	0.05	0.005	−1.496	0.505	1.570	0.506	0.803	0.122
Experimentally-fitted	25	0.072	0.012	0.242	0.092	−1.367	0.015	1.571	0.054	0.810	0.015

primitives [37]. Stulp et al. used a reinforcement learning algorithm and motion primitives to improve the robustness of grasping and pick-and-place tasks [38].

This prior work mainly focused on comparatively simple objects with few degrees-of-freedom, which do not fully account for the true complexity of objects that humans can handle. Flexible objects with highly complex internal dynamics remain particularly challenging for robots. The only comparable study, to our knowledge, demonstrated whip-cracking with a robot manipulator [39]. However, in that study the motion trajectory of the robot was determined by replicating experimental observations of actual human performance. Planning using optimization based on dynamic motor primitives was not considered.

The work reported here also represented the command from the CNS as a stereotyped primitive motion profile but in addition included a simplified (but reasonable) representation of the mechanical impedance of the neuromuscular system. This distinction is important; recent results have shown that humans appear to tune their neuromuscular mechanical impedance when manipulating objects with complex internal dynamics [40].

Biological observations from previous studies were considered in determining the model of the upper limb controller. Although muscle force production is a complex function of many factors, its dominant behavior can well be described by a function of muscle length and its rate of change [23], [41], [42]. The joint torques resulting from activation of relevant muscles were assumed to depend upon the position and velocity deviation between the actual upper limb posture and a "zero-torque" posture. As the upper limb controller was described in relative angle coordinates, the stiffness matrix K was taken to be constant, since it was previously shown that joint stiffness is (approximately) constant in joint coordinates [43]. Based on reports showing that the stiffness field of the upper arm is nearly curl-free and predominantly spring-like, stiffness matrix K was chosen to be symmetric [44]. Consistent with a single time-constant characterizing neuromuscular interactive dynamics, values for the joint damping matrix B were assumed to be proportional to joint stiffness matrix K [23]. This set of observations served as the basis for the upper limb controller used here, yielding a motion which resembled the actual motor behavior of the upper limb.

It is worth noting that the upper limb controller was "ignorant" of the complex whip dynamics. While it is straightforward (albeit tedious) to derive the equations of motion of the $N+2$ degrees-of-freedom model, optimization

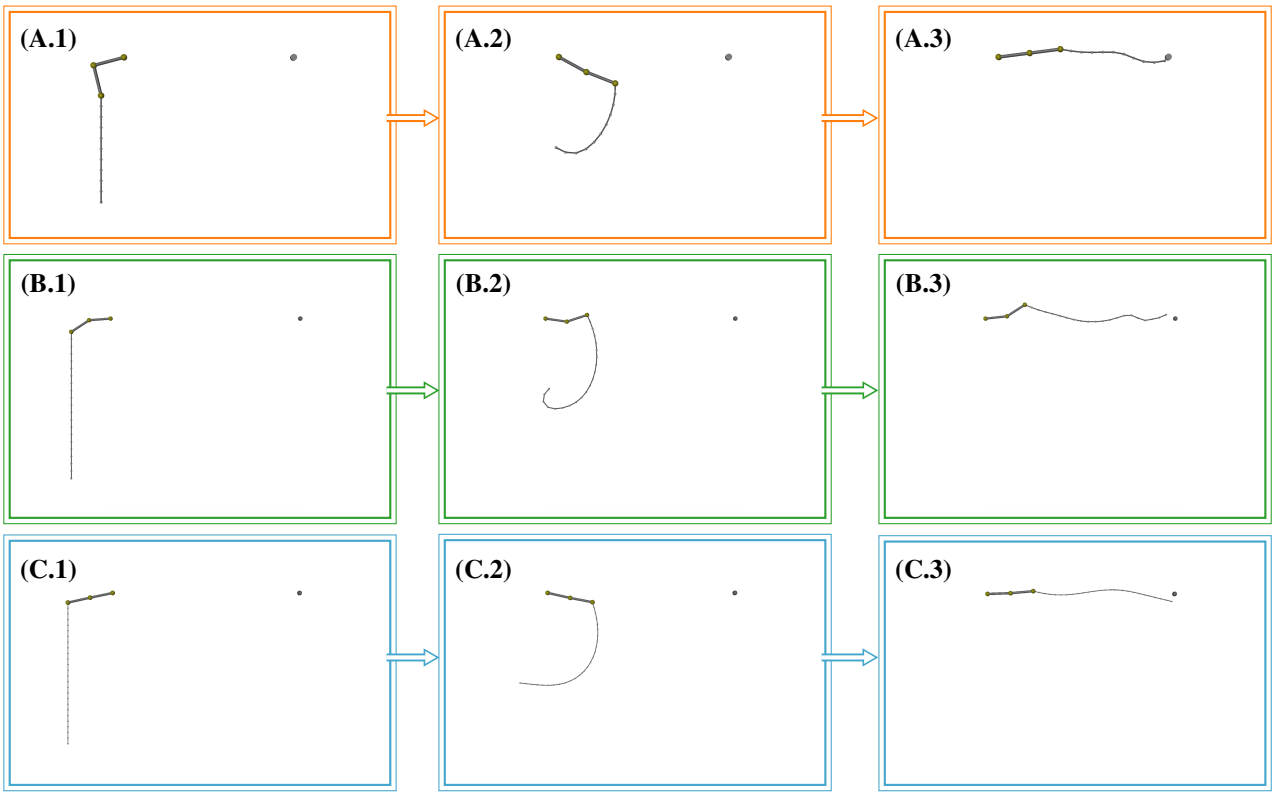

Fig. 3: Time sequence of the simulation of the whip models. (A) Short whip (B) Long whip (C) Experimentally-fitted whip. Each upper limb movement was generated with the optimal movement parameters, which yielded the minimum distance L^*.

using such a complex mathematical model seems impractical, challenging even with modern computational resources. Using dynamic motor primitives, the whip-targeting task was achieved without the need to store or recall any detailed mathematical representation of the whole system dynamics. This approach may be a key simplification required to learn complex motor skills, since only a small set of parameters are acquired and retained. To the extent that dynamic motor primitives offer a simplified solution to complex and flexible object manipulation, this approach may facilitate robotic manipulation of flexible materials, which is presently a major challenge.

B. Limitations

It is notable that the minimum distance for the longest whip was greater than for the short, medium and the experimentally-fitted whip model. This result suggests that a single dynamic primitive may not be sufficient in this case. Adding a second dynamic primitive may improve performance. In fact, observations of a skilled human performer indicate that one action (sometimes rhythmic) is used to "energize" the whip, while a second action (e.g. a "wrist flick") serves to propagate a wave along it [14]. Studying this possibility is a topic of ongoing work.

Simulating the continuous whip dynamics with a finite number of lumped-parameter sub-models enabled a compromise between ease of analysis and fidelity of reproducing essential behavior. Since numerical dissipation acted as intrinsic damping within the simulation, dissipation in the whip model is the sum of the numerical dissipation and the model dissipation (due to non-zero b). Carefully choosing the damping value b may compensate for the numerical error intrinsic to the simulation, such that the combination provides a reliable approximation of actual whip behavior.

In this simulation study, the wrist joint was neglected for simplicity, since it is always better to start simple and slowly add complexity, rather than the other way around. Anecdotally, the wrist appears to play a prominent role in skilled whip manipulation. However, at this time the role of the wrist remains unclear. Future work, extending the arm model to three or more degrees of freedom and extending the whip model to three dimensions, may clarify the role of the wrist.

V. Conclusion

Despite the significant limitations of our neuromuscular system, humans manipulate objects of prodigious dynamic complexity with apparent ease. The simulations presented here showed that encoding control via the parameters of dynamic primitives enabled optimization to identify actions that led to successfully handling an extremely complex dynamic object—a whip. Understanding how this was accomplished may facilitate endowing robots with comparable dexterity.

References

[1] C. M. Keller, J. D. Keller *et al.*, *Cognition and tool use: The blacksmith at work*. Cambridge University Press, 1996.

[2] G. R. Hunt, "Manufacture and use of hook-tools by new caledonian crows," *Nature*, vol. 379, no. 6562, p. 249, 1996.

[3] S. H. Johnson-Frey, "The neural bases of complex tool use in humans," *Trends in Cognitive Sciences*, vol. 8, no. 2, pp. 71–78, 2004.

[4] C. Boesch and H. Boesch, "Tool use and tool making in wild chimpanzees," *Folia Primatologica*, vol. 54, no. 1-2, pp. 86–99, 1990.

[5] B. Kenward, A. A. Weir, C. Rutz, and A. Kacelnik, "Behavioural ecology: Tool manufacture by naive juvenile crows," *Nature*, vol. 433, no. 7022, p. 121, 2005.

[6] E. R. Kandel, J. H. Schwartz, T. M. Jessell, D. of Biochemistry, M. B. T. Jessell, S. Siegelbaum, and A. Hudspeth, *Principles of Neural Science*. McGraw-hill New York, 2000, vol. 4.

[7] D. M. Wolpert, R. C. Miall, and M. Kawato, "Internal models in the cerebellum," *Trends in Cognitive Sciences*, vol. 2, no. 9, pp. 338–347, 1998.

[8] M. Kawato, "Internal models for motor control and trajectory planning," *Current Opinion in Neurobiology*, vol. 9, no. 6, pp. 718–727, 1999.

[9] J. R. Flanagan, P. Vetter, R. S. Johansson, and D. M. Wolpert, "Prediction precedes control in motor learning," *Current Biology*, vol. 13, no. 2, pp. 146–150, 2003.

[10] F. Crevecoeur, J. McIntyre, J.-L. Thonnard, and P. Lefevre, "Movement stability under uncertain internal models of dynamics," *Journal of Neurophysiology*, vol. 104, no. 3, pp. 1301–1313, 2010.

[11] R. Shadmehr and Z. M. Moussavi, "Spatial generalization from learning dynamics of reaching movements," *Journal of Neuroscience*, vol. 20, no. 20, pp. 7807–7815, 2000.

[12] B. Bernstein, D. A. Hall, and H. M. Trent, "On the dynamics of a bull whip," *The Journal of the Acoustical Society of America*, vol. 30, no. 12, pp. 1112–1115, 1958.

[13] A. Goriely and T. McMillen, "Shape of a cracking whip," *Physical Review Letters*, vol. 88, no. 24, p. 244301, 2002.

[14] C. C. I. Henrot, "Characterization of whip targeting kinematics in discrete and rhythmic tasks," Undergraduate Thesis, Massachusetts Institute of Technology, 2016.

[15] A. J. Choi. Slow motion whip jenga. Youtube. [Online]. Available: https://www.youtube.com/watch?v=9J_u_m5XvdA

[16] R. Ronsse, D. Sternad, and P. Lefevre, "A computational model for rhythmic and discrete movements in uni-and bimanual coordination," *Neural Computation*, vol. 21, no. 5, pp. 1335–1370, 2009.

[17] N. Hogan and D. Sternad, "Dynamic primitives of motor behavior," *Biological Cybernetics*, vol. 106, no. 11-12, pp. 727–739, 2012.

[18] ——, "Dynamic primitives in the control of locomotion," *Frontiers in Computational Neuroscience*, vol. 7, p. 71, 2013.

[19] N. Hogan, "Physical interaction via dynamic primitives," in *Geometric and Numerical Foundations of Movements*. Springer, 2017, pp. 269–299.

[20] D. Sternad, "Human control of interactions with objects–variability, stability and predictability," in *Geometric and Numerical Foundations of Movements*. Springer, 2017, pp. 301–338.

[21] E. Todorov, T. Erez, and Y. Tassa, "Mujoco: A physics engine for model-based control," in *2012 IEEE/RSJ International Conference on Intelligent Robots and Systems*. IEEE, 2012, pp. 5026–5033.

[22] H. Hatze, "A mathematical model for the computational determination of parameter values of anthropomorphic segments," *Journal of Biomechanics*, vol. 13, no. 10, pp. 833–843, 1980.

[23] T. Flash, "The control of hand equilibrium trajectories in multi-joint arm movements," *Biological Cybernetics*, vol. 57, no. 4-5, pp. 257–274, 1987.

[24] N. Hogan, "Impedance control: An approach to manipulation: Part ii—implementation," *Journal of Dynamic Systems, Measurement, and Control*, vol. 107, no. 1, pp. 8–16, 1985.

[25] T. Flash and N. Hogan, "The coordination of arm movements: an experimentally confirmed mathematical model," *Journal of Neuroscience*, vol. 5, no. 7, pp. 1688–1703, 1985.

[26] J. M. Gablonsky and C. T. Kelley, "A locally-biased form of the direct algorithm," *Journal of Global Optimization*, vol. 21, no. 1, pp. 27–37, 2001.

[27] J. A. Doeringer and N. Hogan, "Serial processing in human movement production," *Neural Networks*, vol. 11, no. 7-8, pp. 1345–1356, 1998.

[28] N. Hogan, J. A. Doeringer, and H. I. Krebs, "Arm movement control is both continuous and discrete," *Cognitive Studies*, vol. 6, no. 3, pp. 254–273, 1999.

[29] D. Sternad, W. J. Dean, and S. Schaal, "Interaction of rhythmic and discrete pattern generators in single-joint movements," *Human Movement Science*, vol. 19, no. 4, pp. 627–664, 2000.

[30] A. De Rugy and D. Sternad, "Interaction between discrete and rhythmic movements: Reaction time and phase of discrete movement initiation during oscillatory movements," *Brain Research*, vol. 994, no. 2, pp. 160–174, 2003.

[31] T. Flash and B. Hochner, "Motor primitives in vertebrates and invertebrates," *Current Opinion in Neurobiology*, vol. 15, no. 6, pp. 660–666, 2005.

[32] S. Degallier and A. Ijspeert, "Modeling discrete and rhythmic movements through motor primitives: a review," *Biological Cybernetics*, vol. 103, no. 4, pp. 319–338, 2010.

[33] N. Dominici, Y. P. Ivanenko, G. Cappellini, A. d'Avella, V. Mondì, M. Cicchese, A. Fabiano, T. Silei, A. Di Paolo, C. Giannini *et al.*, "Locomotor primitives in newborn babies and their development," *Science*, vol. 334, no. 6058, pp. 997–999, 2011.

[34] A. J. Ijspeert, J. Nakanishi, and S. Schaal, "Movement imitation with nonlinear dynamical systems in humanoid robots," in *Proceedings 2002 IEEE International Conference on Robotics and Automation (Cat. No. 02CH37292)*, vol. 2. IEEE, 2002, pp. 1398–1403.

[35] S. Schaal and D. Sternad, "Programmable pattern generators," in *3rd International Conference on Computational Intelligence in Neuroscience*, Research Triangle Park, NC, Oct. 24-28, Oct. 1998, pp. 48–51, clmc. [Online]. Available: http://www-clmc.usc.edu/publications/S/schaal-ICCIN1998.pdf

[36] S. Schaal, J. Peters, J. Nakanishi, and A. Ijspeert, "Control, planning, learning, and imitation with dynamic movement primitives," in *Workshop on bilateral paradigms on humans and humanoids, IEEE International Conference on Intelligent Robots and Systems*, 2003, pp. 1–21.

[37] J. Peters and S. Schaal, "Policy gradient methods for robotics," in *2006 IEEE/RSJ International Conference on Intelligent Robots and Systems*. IEEE, 2006, pp. 2219–2225.

[38] F. Stulp, E. A. Theodorou, and S. Schaal, "Reinforcement learning with sequences of motion primitives for robust manipulation," *IEEE Transactions on Robotics*, vol. 28, no. 6, pp. 1360–1370, 2012.

[39] Y. Yamakawa, K. Odani, and M. Ishikawa, "Sonic-speed manipulation of a bull whip using a robot manipulator," in *2016 IEEE International Conference on Advanced Intelligent Mechatronics (AIM)*. IEEE, 2016, pp. 1139–1144.

[40] P. Maurice, N. Hogan, and D. Sternad, "Predictability, force, and (anti) resonance in complex object control," *Journal of Neurophysiology*, vol. 120, no. 2, pp. 765–780, 2018.

[41] G. Joyce, P. Rack, and D. Westbury, "The mechanical properties of cat soleus muscle during controlled lengthening and shortening movements," *The Journal of Physiology*, vol. 204, no. 2, pp. 461–474, 1969.

[42] P. M. Rack and D. Westbury, "The effects of length and stimulus rate on tension in the isometric cat soleus muscle," *The Journal of Physiology*, vol. 204, no. 2, pp. 443–460, 1969.

[43] T. Flash and F. Mussa-Ivaldi, "Human arm stiffness characteristics during the maintenance of posture," *Experimental Brain Research*, vol. 82, no. 2, pp. 315–326, 1990.

[44] F. A. Mussa-Ivaldi, N. Hogan, and E. Bizzi, "Neural, mechanical, and geometric factors subserving arm posture in humans," *Journal of Neuroscience*, vol. 5, no. 10, pp. 2732–2743, 1985.